



## Experimental evaluation of CO<sub>2</sub> enhanced recovery of adsorbed-gas from shale



Jun Liu<sup>a,c</sup>, Yanbin Yao<sup>a,\*</sup>, Dameng Liu<sup>a</sup>, Derek Elsworth<sup>b</sup>

<sup>a</sup> Coal Reservoir Laboratory of National Engineering Research Center of CBM Development & Utilization, China University of Geosciences, Beijing 100083, PR China

<sup>b</sup> Department of Energy and Mineral Engineering, Pennsylvania State University, University Park, PA 16802, USA

<sup>c</sup> Shandong Provincial Key Laboratory of Depositional Mineralization & Sedimentary Minerals, Shandong University of Science and Technology, Qingdao, Shandong 266590, China

### ARTICLE INFO

#### Keywords:

Shale gas  
CO<sub>2</sub>-EGR (enhance gas recovery)  
Adsorbed-phase methane  
Low-field NMR  
Jiaoshiiba shale gas field

### ABSTRACT

Existing methods for shale reservoir stimulation (e.g., hydraulic fracturing) focus mainly on improving the physical recovery of free phase gases from shales. Few studies explore the enhanced recovery of adsorbed methane from shale due to the difficulty in simultaneously separating the recovery of both the adsorbed and free phase gas. In this study, we use an NMR-based methodology to separately evaluate the change in adsorbed and non-adsorbed (free-phase) methane during the injection of CO<sub>2</sub>. We evaluate mechanisms contributing to the enhanced recovery of adsorbed-gas with CO<sub>2</sub> injection (Longmaxi shale, Jiaoshiiba field, SW China). Results show that the injection of CO<sub>2</sub> can improve the efficiency of recovery of residual gas in the adsorbed phase by an additional ~25% and can enhance the percent recovery per hour of adsorbed methane by ~11% at ambient pressure and ~4% at abandonment pressure. The experiments also demonstrate that a higher concentration ratio of CO<sub>2</sub>/CH<sub>4</sub> is more suitable for CO<sub>2</sub>-CH<sub>4</sub> displacement, and the CO<sub>2</sub>-CH<sub>4</sub> displacement rate is relatively rapid during the early phase of interaction, immediately after injection. Despite inherent uncertainty, these experiments demonstrate the capability of enhancing adsorbed-gas recovery by injection of CO<sub>2</sub> into shale.

### 1. Introduction

Shales are fine-grained clastic sedimentary rocks formed by the compaction of predominately clay-sized materials, including both mineralogical and organic materials (Goodman et al., 2014). Generated methane is mainly stored as a free phase gas (non-adsorbed) in fractures and matrix pores, as an adsorbed component on kerogen and clay surfaces, and possibly in the dissolved phase in formation fluids (Vermylen, 2011; Rani et al., 2015). Production of shale gas has from such unconventional reservoirs been successful due to advances in horizontal drilling and hydraulic fracturing technologies (Eshkalak et al., 2014). However, the present shale gas plays commonly show extremely high decline rates (63% per year and more) of gas production (Sandrea, 2012), due to the fact that most gas production is contributed from free phase gases in shales. Except free gas, there are large amount of adsorbed phase gases in shale gas reservoirs. Thus, for enhancing commercial shale gas production greatly, it is extremely important to improve the recovery of adsorbed phase gases. Unfortunately, this topic is not well investigated in existing researches. The main focus of this study is to demonstrate possibility of enhancing gas recovery (EGR) of adsorbed phase gases in shale reservoirs.

Enhanced coalbed methane recovery with injected CO<sub>2</sub> has been investigated in several coal fields with positive outcomes (Chen et al., 2010; Busch and Gensterblum, 2011). For example, CO<sub>2</sub> injection improved methane recovery from 77% to 95% of the original gas-in-place in the San Juan Basin, USA (Reeves, 2004). Similar to coal, kerogen and clays within gas shales possess large surface areas and have significant gas adsorption capacity not only for CH<sub>4</sub> but also for CO<sub>2</sub> (Godec et al., 2013; Goodman et al., 2014). Gas shales exhibit a significant preferential adsorption of CO<sub>2</sub> over CH<sub>4</sub> (Nuttall et al., 2005), making it possible to enhance methane recovery by the injection of CO<sub>2</sub>, this potential being affirmed for CO<sub>2</sub> storage in the Marcellus shale (Godec et al., 2014). Enhanced gas recovery may be symbiotically paired with Carbon Capture and Storage in shale gas reservoirs (Chu and Majumdar, 2012; Harrison and Falcone, 2013).

Recent studies in enhancing gas/oil recovery by injection of CO<sub>2</sub> into shales have demonstrated increases in the rate and the volume of CH<sub>4</sub> recovered (Regan, 2007). The injected CO<sub>2</sub> can be trapped in shale in the adsorbed phase with the parallel displacement of CH<sub>4</sub>. For the same shale sample, CO<sub>2</sub> may have an adsorption capacity approximately 2–5 times greater than that of CH<sub>4</sub> (Nuttall et al., 2005; Heller and Zoback, 2014). Reservoir simulation research by Liu et al. (2013)

\* Corresponding author.

E-mail address: [yyb@cugb.edu.cn](mailto:yyb@cugb.edu.cn) (Y. Yao).

also demonstrated that the potential for CO<sub>2</sub> to displace CH<sub>4</sub> by up to a 5:1 molecular ratio. The continuous injection of CO<sub>2</sub> over a period of 45 days (Scheepers et al., 2009) may result in significant improvement in shale gas recovery. This may result in an enhanced recovery factor of original oil in place (OOIP) from 10% to 55% after injection of CO<sub>2</sub> (Ferno et al., 2015) and this may be demonstrated theoretically in also improving gas recovery in shale gas reservoirs (Sun et al., 2013; Fathi and Akkutlu, 2014). However, few experimental studies have explored the efficiency, the internal mechanism, and the dynamic process of CO<sub>2</sub>-EGR in shale gas reservoirs.

Nuclear Magnetic Resonance (NMR) provides a fast, convenient and non-destructive detection method to investigate hydrogen-bearing fluid-phases (e.g., water and methane) in porous media. This method has been commonly used in the petrophysical characterization of reservoir rocks (Yao et al., 2010; Fleury and Romero-Sarmiento, 2016; Li et al., 2017), oil/gas saturation (Sigal and Odusina, 2011), methane adsorption capacity (Guo et al., 2007; Yao et al., 2014), and the interactions of CO<sub>2</sub> and H<sub>2</sub>O in coals (Sun et al., 2016). Nevertheless, the application of NMR to probe important behaviors in shale gas recovery is relatively uncharted. This study used NMR in a first attempt to investigate the dynamic fluid interactions/exchange process between adsorbed methane and injected CO<sub>2</sub>. This is important in evaluating the potential to enhance adsorbed-gas recovery with CO<sub>2</sub> injection in shale gas reservoirs.

## 2. Materials and analytical methodology

### 2.1. Shale sample

A sample of black shale core was collected from the Lower Silurian Longmaxi Formation (southeastern Sichuan basin) at a depth of 1072 m. The sampled well is located in the Jiaoshiha shale gas field, the most successful shale gas production area in China. The shale sample has high TOC content (4.57%) and high thermal maturity ( $R_o$  of 2.77%). Minerals in the sample are dominated by quartz and clay minerals, a few carbonate minerals and feldspar, and negligible pyrite (Table 1). The clay minerals are mainly the illite and illite-smectite mixed-layer minerals, with negligible chlorite, while the carbonate minerals are composed of dolomite, calcite, and siderite (Table 1).

The pores in the shale sample are mainly the organic pores, interparticular pores, and some microfractures (Fig. 1). The pore type of the shale is dominated by micropores (< 10 nm) with typical pore morphology of “ink bottle pore” (Fig. 2). Nano-pores are well developed in the shale sample (Fig. 2), which resulted in high pore surface area of the shale sample (25.1788 m<sup>2</sup>/g) (Table 1).

### 2.2. Experimental setup

The principal experimental setup consists of an NMR measurement apparatus, a core holder, a high-pressure gas supply system, a one-way release valve and an exhaust device (Fig. 3). The NMR measurement apparatus contains a 60 mm diameter magnet coil that creates a homogeneous internal field gradient. The core holder confines the sample and is sealed during the experiments. These components are

**Table 1**  
Detailed information of the study shale sample.

TOC (%)	$R_o$ (%)	Low-pressure N <sub>2</sub> adsorption analysis <sup>a</sup>			Mineral composition (wt%) <sup>b</sup>				
		$S$ (m <sup>2</sup> /g)	$V$ (cm <sup>3</sup> /g)	$r$ (nm)	Q	Cly	C	F	Py
4.57	2.77	25.1788	0.0172	5.7186	47.2	34.3	9.3	7.9	1.3

Clay minerals (Cly) including 58% illite-smectite mixed-layer mineral, 38% illite, and 4% chlorite. Carbonate minerals (C) are composed of 68.8% dolomite, 22.6% calcite and 8.6% siderite.

<sup>a</sup>  $S$ ,  $V$ ,  $r$  are the BET pore surface area, BJH total pore volume shale, and average pore size, respectively.

<sup>b</sup> Q – quartz; Cly – clay minerals; C – carbonate minerals; F – feldspar; Py – pyrite.

custom-designed with nonmagnetic and nonmetallic materials in the segment located within the magnet coil. The high-pressure gas supply system includes two gas cylinders (CH<sub>4</sub>, CO<sub>2</sub>), a booster pump and a vacuum pump. A one-way release valve is used to ensure that the gas fluid can pass only from the sample cell directly to the exhaust. Transducers monitor the gas pressure and temperature in real time.

### 2.3. Low-field NMR measurements

The low-field NMR measurement method uses the <sup>1</sup>H nuclear magnetic resonance phenomenon in a uniform magnetic field to analyze rock porosity and/or fluid characteristics in the porous medium (Hazlewood et al., 1974). Only fluids containing hydrogen, such as CH<sub>4</sub> and H<sub>2</sub>O, exhibit NMR relaxation; hydrogen-free fluids, such as CO<sub>2</sub> and He, have no NMR signal, making it possible to analyze CH<sub>4</sub> displacement by CO<sub>2</sub>.

The number of hydrogen atoms present in the CH<sub>4</sub> can be detected by using a transverse ( $T_2$ ) relaxation time measurement (Seevers, 1966). The  $T_2$  distributions were measured using Carr, Purcell, Meiboom and Gill (CPMG) pulse sequences (Carr and Purcell, 1954; Meiboom and Gill, 1958). The measurement of the sample was performed using a 23.15 MHz NMR spectrometer. The  $T_2$  distributions were generated using inverse Laplace non-negative least square fitting echo train data (Buttler et al., 1981). The smoothing parameter was calculated using the methodology described by Dunn et al. (1994).

The total signal amplitude from a typical  $T_2$  distribution measurement is represented by the complete relaxation equation:

$$\frac{1}{T_2} = \frac{1}{T_{2B}} + \frac{1}{T_{2S}} + \frac{1}{T_{2D}} \quad (1)$$

where  $T_{2B}$ ,  $T_{2S}$  and  $T_{2D}$  represent bulk, surface, and diffuse relaxation, respectively.

In this study, the magnetic uniformity is as low as 30 ppm, so that the relaxation caused by gas diffusion can be neglected. This means that value of  $\frac{1}{T_{2D}}$  is sufficiently small (Yao et al., 2014), to be neglected in Eq. (1) under the experimental conditions. Thus, Eq. (1) becomes

$$\frac{1}{T_2} = \frac{1}{T_{2B}} + \frac{1}{T_{2S}} + \frac{1}{T_{2B}} + \rho \frac{S}{V} \quad (2)$$

where  $\rho$  is the surface relaxivity and  $S/V$  is the surface-to-volume ratio of the pore. The relaxations of methane in shale sample include bulk relaxation ( $T_{2B}$ ) of non-adsorbed methane gas and surface relaxation ( $T_{2S}$ ) of adsorbed methane gas. The  $T_{2B}$  is related to the specific density (or molarity) of non-adsorbed methane gas (Seevers, 1966), whereas the  $T_{2S}$  is directly related to relaxivity and pore structure. The total signal amplitude for a  $T_2$  distribution is closely tied to the number of <sup>1</sup>H protons of the adsorbed methane and non-adsorbed methane gases.

### 2.4. Experimental procedures

Prior to the NMR measurements, the collected shale sample was crushed and sieved into fine fragments with a diameter of ~3 mm. Using the same sample, we conducted a sequential series of four NMR experiments, to examine Processes A1, A2, B1 and B2, as shown in

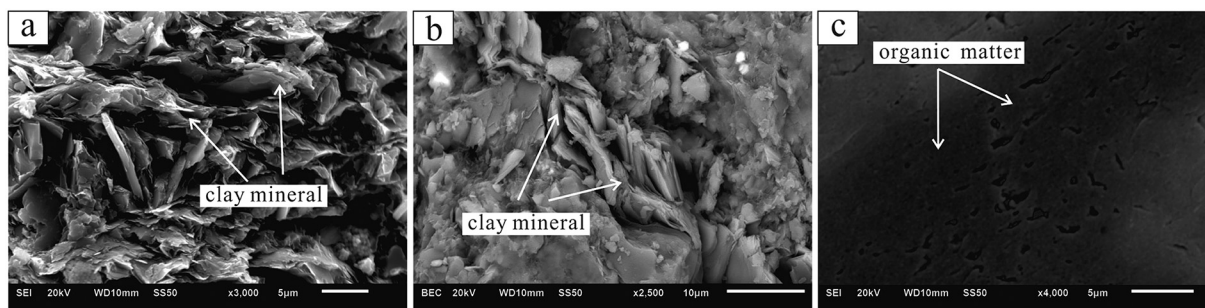


Fig. 1. Pores in collected shale samples observed by SEM.

Fig. 4. At the beginning of each process, the shale fragments were dried at constant temperature (110 °C for 1 h) in a dry container to remove moisture and then immediately transferred to sample cell to vacuumize for 2 h to desorb the adsorbed gases in the shale. The shale was then fully saturated with CH<sub>4</sub> at a gas pressure of 6 MPa (Fig. 4). The remaining operations for each experimental process are shown in Fig. 4, and the details are given below.

The purpose of Processes A1 and A2 (Fig. 4) was to compare the desorption characteristics between natural desorption (without CO<sub>2</sub> injection) and desorption with the infusion of CO<sub>2</sub> at 4.5 MPa (total pressure in cell), with the sample cell depressurized to ambient pressure (approximate 0.1 MPa). Processes B1 and B2 (with CO<sub>2</sub> injection) were designed to compare natural desorption (without CO<sub>2</sub> injection) with desorption at injection pressures of 4.5 MPa CO<sub>2</sub> (total pressure in cell), with the sample cell depressurized to reservoir abandonment pressure. In this study, the reservoir abandonment pressure was defined as 1.5 MPa (Zhang et al., 2015). Moreover, Process A1 and Process B1 are used to investigate the difference between the natural desorption capacity of adsorbed CH<sub>4</sub> at ambient pressure versus that at abandonment pressure. In addition, Process A2 and Process B2 are used to explore the influence of injected CO<sub>2</sub> on the recovery efficiency of adsorbed CH<sub>4</sub>.

Except for the oven-drying of samples, all other experimental operations were conducted under a constant temperature of 35 °C. We chose the temperature of 35 °C but not a higher temperature (e.g. in-situ temperature of 60–65 °C) because high temperature can bring disturb of the NMR measurement results, due to the limitation of the selected NMR spectrometer in this study. For each decompression operation, the speed and rate of decompression remained constant. During the processes of CH<sub>4</sub> saturation, CH<sub>4</sub> desorption, and CH<sub>4</sub> displacement by CO<sub>2</sub> injection, NMR measurements were recorded at 1.5 h intervals, until two successive measurements exhibited negligible difference.

### 3. Results and discussions

#### 3.1. Evaluation of non-adsorbed gas content based on NMR measurements

For non-adsorbed methane (i.e., bulk methane), the specific density

(or molarity) can be obtained by performing a series of NMR measurements on non-adsorbed methane at different pressures (see Yao et al. (2014) for details). In this study, we conducted NMR measurements for bulk methane at 35 °C, and under gas pressures of 0.77, 2.00, 2.83, 3.45, 4.23, 5.16, and 6.27 MPa. As shown in Fig. 5a, the measure T<sub>2</sub> spectrum amplitude is proportional to the methane pressure. Since the signal amplitude for a given T<sub>2</sub> distribution is closely tied to the number of <sup>1</sup>H protons present, and thus should increase linearly with molecule mass of methane. Fig. 5b shows the linear relationship between amplitude and methane mass. The relationships are expressed as:

$$V_B = 2.884 \times 10^{-5} \times T_B \quad (R^2 = 0.981) \quad (3)$$

where T<sub>B</sub> is the signal amplitude of the measured T<sub>2</sub> for non-adsorbed methane, V<sub>B</sub> represents the non-adsorbed CH<sub>4</sub> content (unit: mol). Eq. (3) can be used to quantify the change of non-adsorbed methane during the CO<sub>2</sub>-CH<sub>4</sub> interaction in shales.

#### 3.2. Evaluation of adsorbed gas content based on NMR measurements

The quantification of the adsorbed gas content based on NMR measurements is extremely important for this study. Some researchers ever provided some methods to quantify the adsorbed methane in coals. Guo et al. (2007) used the amplitude index from bulk methane to quantify the mass and volume of adsorbed methane, which has proven to be problematic in Yao et al. (2014). It is because that the relaxation property of bulk methane is completely different from that of adsorbed methane. Yao et al. (2014) built an NMR transparent isotherm adsorption experimental setup and conducted isothermal adsorption measurements using both the volumetric and NMR methods. They used the adsorbed gas volume that is calculated from the volumetric method to establish a relationship with the amplitude of NMR signals from adsorbed methane. Furtherly, they use the relationship to evaluation of adsorbed gas content of coal (Yao et al., 2014). Yao et al. (2014)'s method is applicable and their results are believable. However, this method needs a paralleling contrast experiment from volumetric method. In this study, we provide a directly quantification method for calculating gas adsorption based on a core flooding and gas adsorption

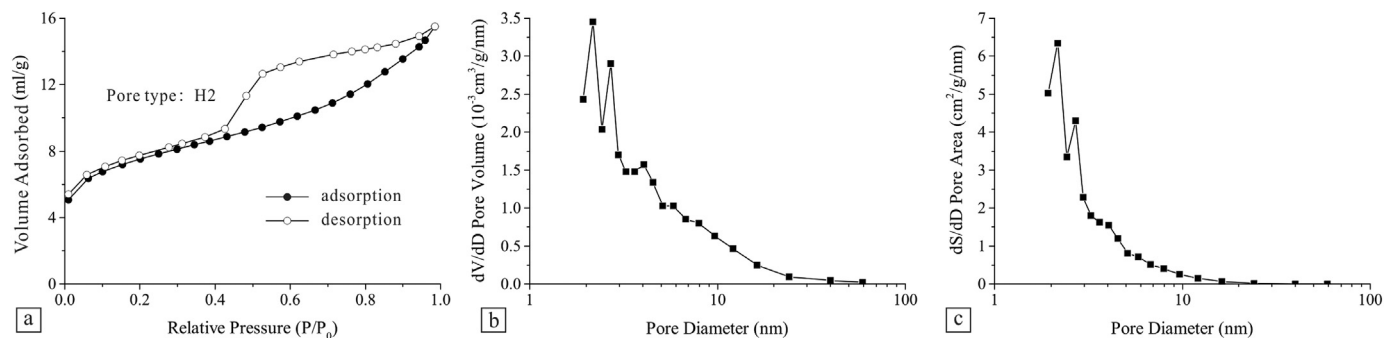


Fig. 2. Typical N<sub>2</sub> adsorption/desorption results at a low temperature (77 K) for study shale sample. (a), Nitrogen adsorption/desorption curve at a low temperature. (b), Distribution curves of the BJH pore volume in different stages. (c), Distribution curves of the BET specific area in the different stages.

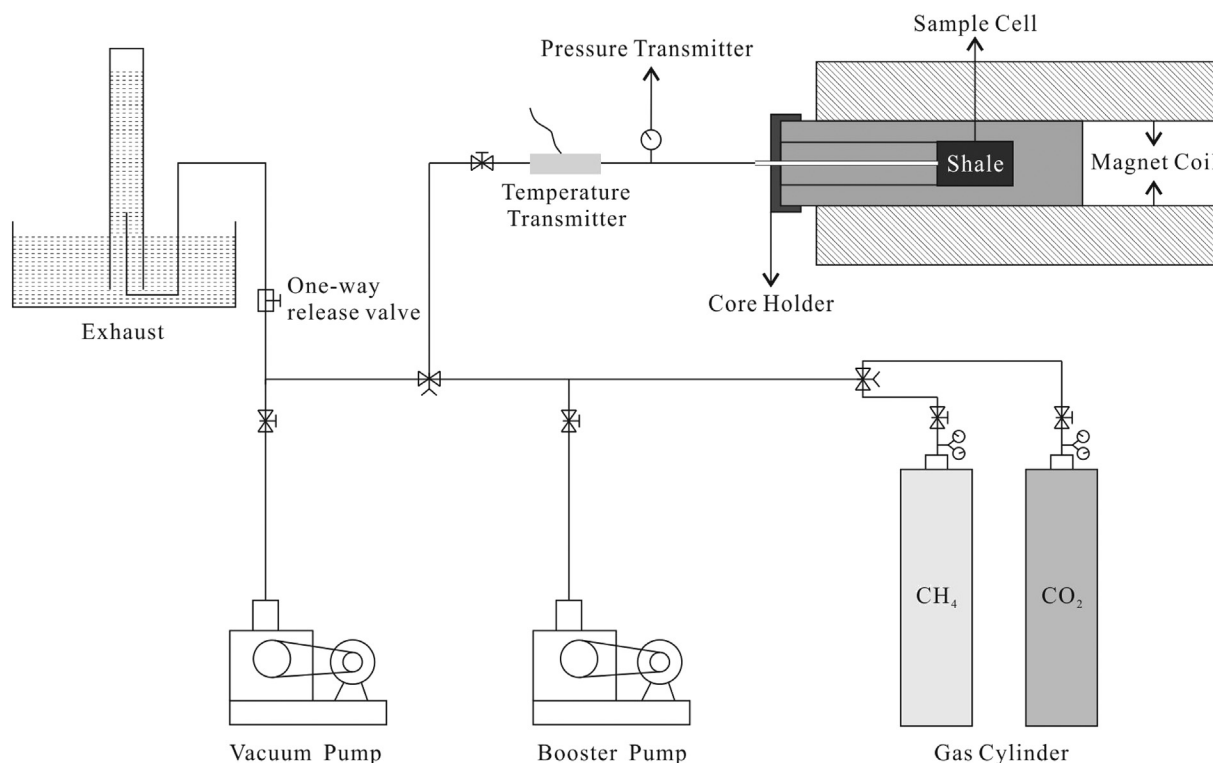


Fig. 3. NMR experimental setup for CO<sub>2</sub>-EGR experiments.

experiment. The method is founded for shale, but is also applicable for coal or other adsorbing materials.

A typical gas adsorption experiment is actually a core flooding process. After initial flooding, the free gas (non-adsorbed) is converted to an adsorbed phase. Using the NMR measurements of Process A2 as an example, the  $T_2$  spectra exhibit three distinctive peaks (Fig. 6). The P1 peak represents the adsorbed gas, while the P2 and P3 peaks represent the non-adsorbed methane (Yao et al., 2014). Only CH<sub>4</sub> (both adsorbed and free-gas/non-adsorbed) were initially present in the sealed cell since the sample was dried and evacuated. As a result, the incremental change in non-adsorbed CH<sub>4</sub> must be exclusively sourced from the adsorbed CH<sub>4</sub>, and vice versa. In other words, the total amount of substance (AOS) of CH<sub>4</sub> characterized by the variation of P2 + P3 amplitudes must be equal to the AOS of CH<sub>4</sub> represented by the change

in P1 amplitude. This can be expressed as.

$$\Delta V_{P1} = \Delta V_{P2+P3} \tag{4}$$

where  $\Delta V_{P1}$  is the incremental (or reduced) AOS of adsorbed CH<sub>4</sub>, while  $\Delta V_{P2+P3}$  indicates the reduced (or incremental) AOS of non-adsorbed CH<sub>4</sub>. Both the  $\Delta V_{P1}$  and  $\Delta V_{P2+P3}$  are in units of mols.

Table 2 gives an example of how the variation of adsorbed CH<sub>4</sub> and non-adsorbed CH<sub>4</sub> were quantified using Process A2. Upon the injection of CO<sub>2</sub> (marked as 0 h in Table 2), the P2 + P3 amplitude varied from 3869.7 p.u. to 4202.4 p.u. ( $\Delta T_{2(P2+P3)}$  is 332.7 p.u.). 332.7 p.u. corresponds to the incremental non-adsorbed CH<sub>4</sub> ( $\Delta V_{P2+P3}$ ) of 0.00962 mol according to Eq. (3). This also suggests the reduction in adsorbed CH<sub>4</sub> (i.e.,  $\Delta V_{P1}$ ) was also 0.00962 mol, which corresponds to the change of P1 amplitude from 453.1 p.u. to 357.3 p.u. ( $\Delta T_{2(P1)}$  is

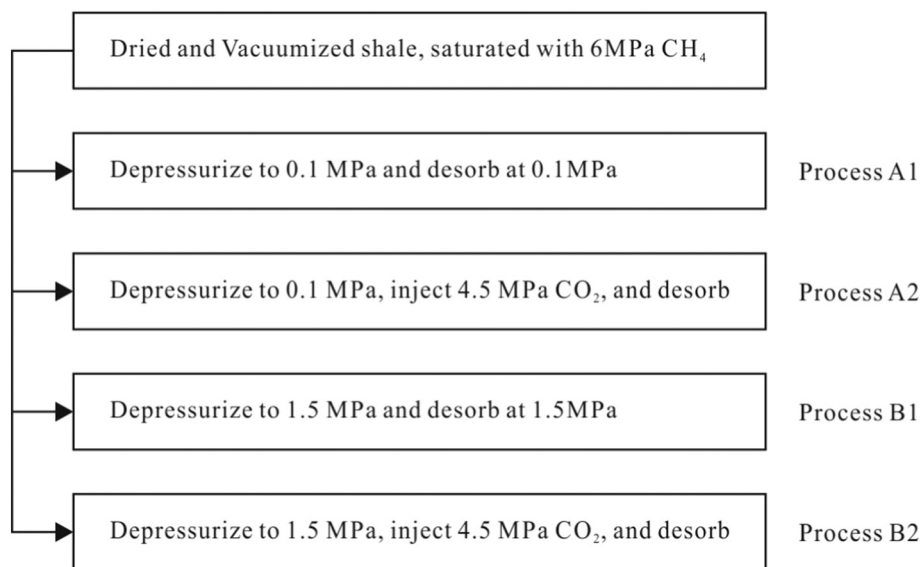


Fig. 4. Flow diagram of experimental processes (4.5 MPa is the total pressure within the sample cell).

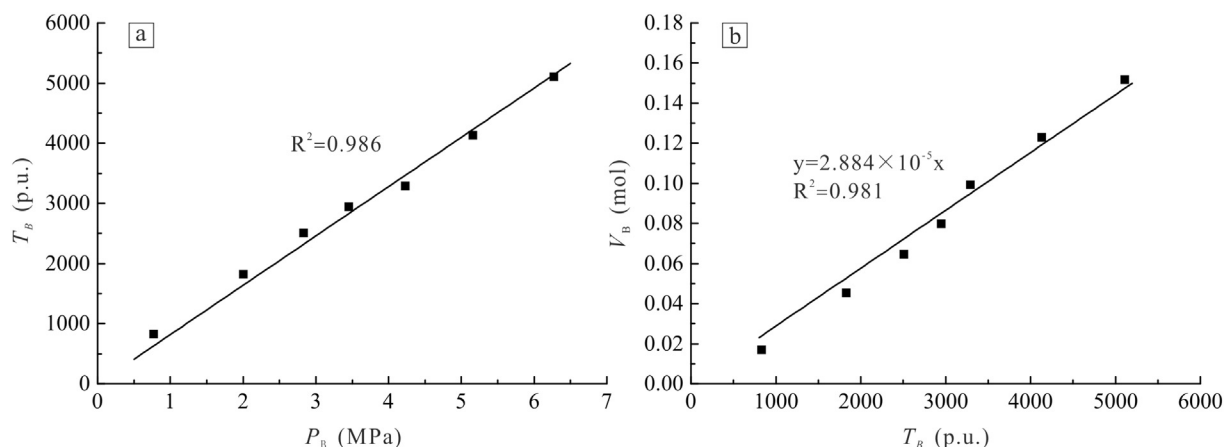


Fig. 5. Relationship between (a) experimental pressure ( $P_b$ ) vs. total  $T_2$  amplitude ( $T_b$ ) and (b) total  $T_2$  amplitude ( $T_b$ ) vs. bulk methane content ( $V_b$ ).

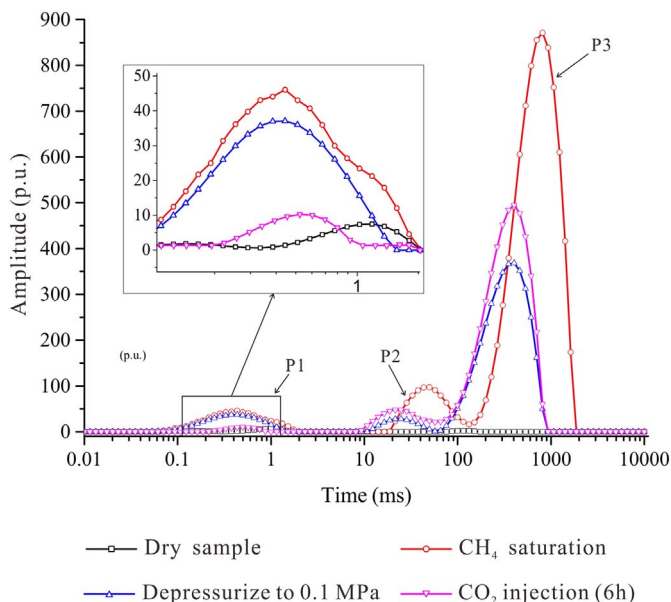


Fig. 6.  $T_2$  spectra of  $CH_4$  in different phases during Process A2.

95.8 p.u.). As a result, a calibration relating  $\Delta T_{2(P1)}$  vs.  $\Delta V_{P1}$  was obtained. During Process A2, a total of five groups of  $\Delta T_{2(P1)}$  vs.  $\Delta V_{P1}$  were obtained, and are given in Table 2. The  $\Delta T_{2(P1)}$  vs.  $\Delta V_{P1}$  relationship is linear (Fig. 7) as:

$$\Delta V_{P1} = 9.792 \times 10^{-5} \times \Delta T_{2(P1)} \quad (R^2 = 0.998) \quad (5)$$

where  $\Delta T_{2(P1)}$  is the change of P1 amplitude, while the  $\Delta V_{P1}$  is the corresponding AOS variation of adsorbed  $CH_4$ .

Eq. (5) can also be written as.

$$V_{P1} = 9.792 \times 10^{-5} \times T_{2(P1)} \quad (R^2 = 0.998) \quad (6)$$

Table 2

Variation of  $T_2$  amplitude and the corresponding AOS of  $CH_4$  in different phases during Process A2.

	Non-adsorbed methane (P2 + P3)				Adsorbed methane (P1)			
	$T_2$ (beginning) (p.u.)	$T_2$ (ending) (p.u.)	$\Delta T_{2(P2+P3)}$ (p.u.)	$\Delta V_{P2+P3}$ (mol)	$T_2$ (beginning) (p.u.)	$T_2$ (ending) (p.u.)	$\Delta T_{2(P1)}$ (p.u.)	$\Delta V_{P1}$ (mol)
0 h	3869.7	4202.4	332.7	0.00962	453.1	357.3	95.8	0.00962
0–1.5 h	4202.4	4723.7	521.3	0.01501	357.3	202.8	154.5	0.01501
1.5–3.0 h	4723.7	4834.4	110.7	0.00322	202.8	171.9	30.9	0.00322
3.0–4.5 h	4834.4	4906.2	71.8	0.00204	171.9	152.4	19.5	0.00204
4.5–6.0 h	4906.2	5182.8	276.6	0.00792	152.4	69.2	83.2	0.00792

Note: 0 h represents the moment of  $CO_2$  injection. The  $T_2$  amplitudes are from the NMR measurements shown in Fig. 6.  $\Delta V_{P2+P3}$  were calculated using Eq. (3).

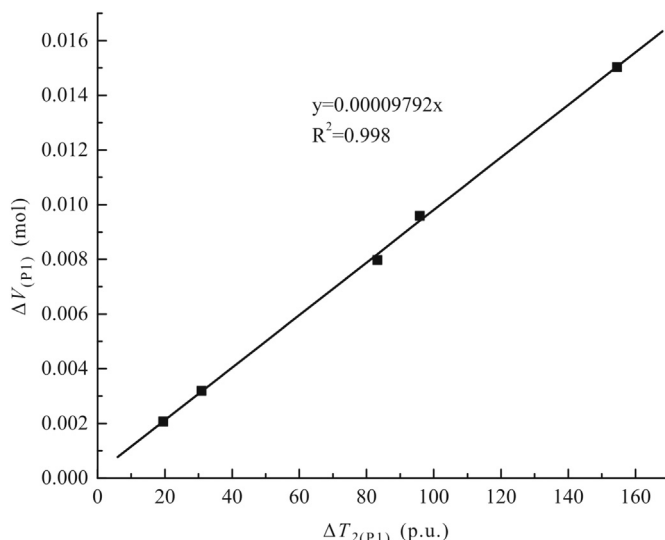


Fig. 7. The linear relationship between  $\Delta T_{2(P1)}$  and  $\Delta V_{P1}$ .  $\Delta T_{2(P1)}$  is the change of P1 amplitude, while  $\Delta V_{P1}$  is the corresponding AOS variation of adsorbed  $CH_4$ . Source data used in this figure are given in Table 2.

where  $T_{2(P1)}$  represents the P1 amplitude and  $V_{P1}$  is the corresponding AOS of adsorbed  $CH_4$ .

Eq. (6) shows that the AOS of adsorbed  $CH_4$  can be calculated from the P1 amplitude. Using Eqs. (3) and (6), the AOS variation of adsorbed  $CH_4$  and non-adsorbed  $CH_4$  in different experimental processes were calculated.

### 3.3. Desorption of adsorbed gas both with and without injected $CO_2$ at ambient pressure

As shown in Process A1 (Fig. 8) and Process A2 (Fig. 6), when the

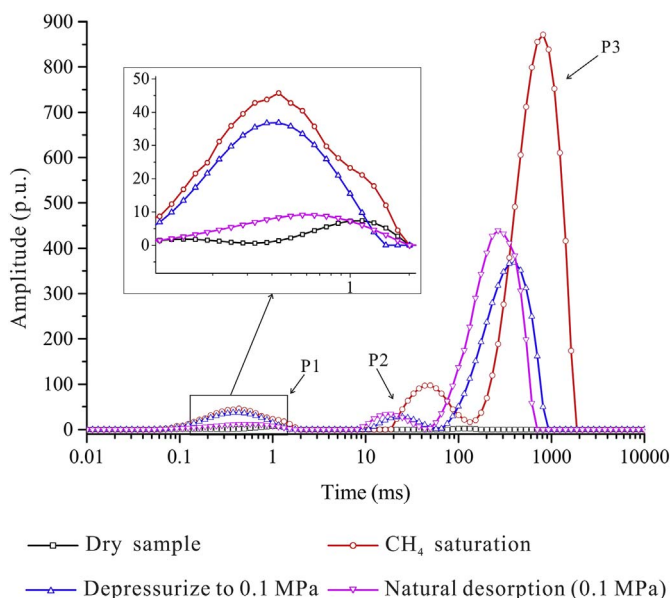


Fig. 8.  $T_2$  spectra of  $CH_4$  in different phases during Process A1.

sample cell was depressurized to ambient pressure, the amplitudes of peaks of P1, P2 and P3 steadily decreased, indicating the desorption of adsorbed methane and release of non-adsorbed methane gases. The reduced amplitude of P1 is lower than that of P2 and P3, suggesting that the desorption of the adsorbed methane lagged the release of non-adsorbed  $CH_4$  during the decompression process.

In this study, we defined the ‘desorption efficiency’ and ‘percent recovery per hour (PRPH)’ to quantify the methane desorption processes. The desorption efficiency is the percentage of the total desorbed mass amount relative to the original adsorbed mass that is present at the moment of  $CO_2$  injection, whereas the PRPH represents the average desorption efficiency per hour. For Process A1, the complete desorption of adsorbed  $CH_4$  required approximately 19.5 h, and the AOS of adsorbed  $CH_4$  varied from 0.0444 mol to 0.0188 mol (Fig. 9a). Thus, the desorption efficiency was 57.66% (Fig. 10a) and the PRPH was 2.96% (Fig. 10b) for the adsorbed  $CH_4$ .

For Process A2, after  $CO_2$  injection, adequate  $CO_2$ - $CH_4$  displacement required 6 h, and the AOS of adsorbed  $CH_4$  varied from 0.0444 mol to 0.0068 mol (Fig. 9a). This demonstrates that a total of 84.68% (Fig. 10a) of adsorbed  $CH_4$  had been desorbed with the injected  $CO_2$  and the PRPH for adsorbed  $CH_4$  was 14.11% (Fig. 10b). Compared with Process A1, injected  $CO_2$  desorbed an additional 27.02% of adsorbed  $CH_4$  (Fig. 10a) and caused the PRPH for adsorbed  $CH_4$  to increase by 11.15% in Process A2 (Fig. 10b).

### 3.4. Desorption of adsorbed gas both with and without injected $CO_2$ at abandonment pressure

In the decompression processes B1 and B2, the P1 amplitude

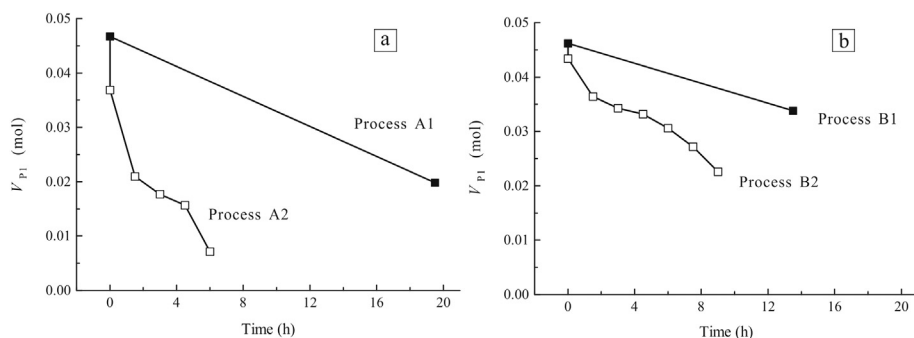


Fig. 9. The AOS variation of adsorbed  $CH_4$  during different experimental processes.  $V_{p1}$  represents the AOS of adsorbed  $CH_4$ . Data were calculated from the NMR measurements per Eq. (6).

exhibits a weak decrease while the amplitudes of both P2 and P3 decrease substantially (Fig. 11, Fig. 12). This indicates that the mass of adsorbed  $CH_4$  decreased slightly but the non-adsorbed  $CH_4$  suffered a significant loss during the decompression process.

In Process B1, the complete desorption of the adsorbed  $CH_4$  at 1.5 MPa required 13.5 h where the AOS of the adsorbed  $CH_4$  reduced from 0.0462 mol to 0.0338 mol (Fig. 9b). This suggests that 26.84% (Fig. 10a) of adsorbed  $CH_4$  had desorbed and the PRPH was 1.99% (Fig. 10b).

In Process B2, an adequate  $CO_2$ - $CH_4$  displacement process required 9 h. After sufficient  $CO_2$ - $CH_4$  interaction, the residual AOS of adsorbed  $CH_4$  was 0.0226 mol, while it was 0.0462 mol at the moment of  $CO_2$  injection (Fig. 9b). Thus the desorption efficiency is 51.08% and the PRPH 5.68% for the adsorbed  $CH_4$ . This demonstrates that the desorption efficiency was improved by 26.24% and the PRPH was enhanced by 3.69% for the adsorbed  $CH_4$  with the  $CO_2$  injected in Process B2 when compared to Process B1 (Fig. 10a, b).

### 3.5. Mechanism of displacement of adsorbed methane by injected $CO_2$

In this study, the non-adsorbed/free-gas  $CH_4$  includes that in large pores and fractures (P2) and the  $CH_4$  in the free space between shale particles or within the sample cell (P3) (Yao et al., 2014). According to Eqs. (3) and (6), the change in P1, P2 and P3 amplitudes directly represent the change of the adsorbed, porous-medium-confined, and free methane in the sample cell, respectively.

Fig. 13 shows the amplitude changes of the three peaks (P1, P2 and P3) after  $CO_2$  injection during Processes A2 and B2. After  $CO_2$  injection, the amplitude of P1 decreases, but the amplitudes of both P2 and P3 increase (Fig. 13). For the P1 amplitude, a decreasing rate was apparent during the two stages of the  $CO_2$ - $CH_4$  interaction: rapid during the first 1.5 h but slowing after 1.5 h (Fig. 13). During the  $CO_2$ - $CH_4$  interaction, some adsorbed  $CH_4$  was driven into the non-adsorbed/free-gas phase because some of the free  $CO_2$  was adsorbed and occupied some of the adsorption sites available for the adsorbed  $CH_4$ . In the previous 1.5 h, the displacement of  $CH_4$  by the free-gas  $CO_2$  was relatively faster than during the remaining time. The P2 amplitude exhibits a relatively weak rate increase during the  $CO_2$ - $CH_4$  interaction (Fig. 13), indicating that only some desorbed  $CH_4$  within the micropores desorbed and diffused into the mesopores and macropores. The P3 amplitude experienced a rapid increase during the first 1.5 h, followed by a steady increase after 1.5 h (Fig. 13), - the opposite trend exhibited in that of P1. This suggests that a major portion of the  $CH_4$  desorbed from adsorbed-phase and was driven into totally free-phase  $CH_4$ , indicating a distinct improvement in gas desorption and related extraction effects (provided high permeabilities may be maintained in stressed media).

As discussed previously, the total pressure in the sample cell was 0.1 MPa of  $CH_4$  for Process A2 and 1.5 MPa of  $CH_4$  for Process B2 before  $CO_2$  injection, while it was 4.5 MPa for both A2 and B2 after  $CO_2$  injection. This means that after  $CO_2$  injection, the original concentration ratio of  $CO_2/CH_4$  in Process A2 was higher than that in Process B2, which is the main reason that desorption efficiency and the PRPH for

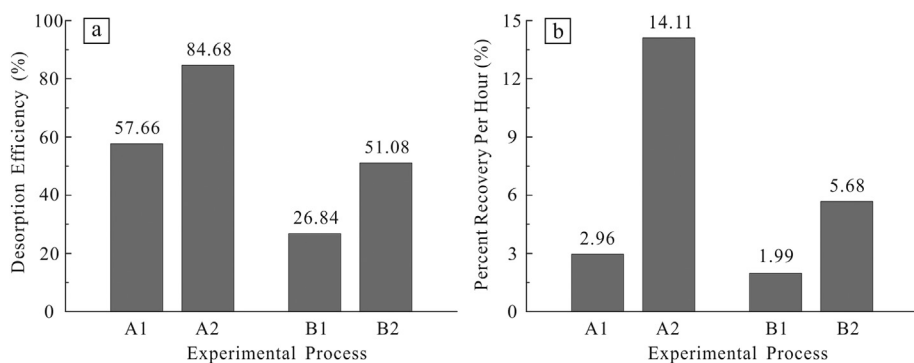


Fig. 10. The desorption efficiency (a) and percent recovery per hour (b) for adsorbed gas in different experimental processes.

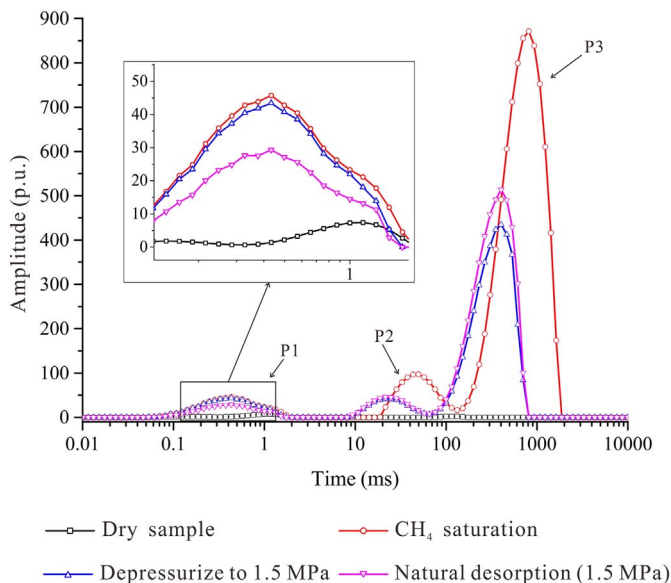


Fig. 11.  $T_2$  spectra of  $CH_4$  in different phases during Process B1.

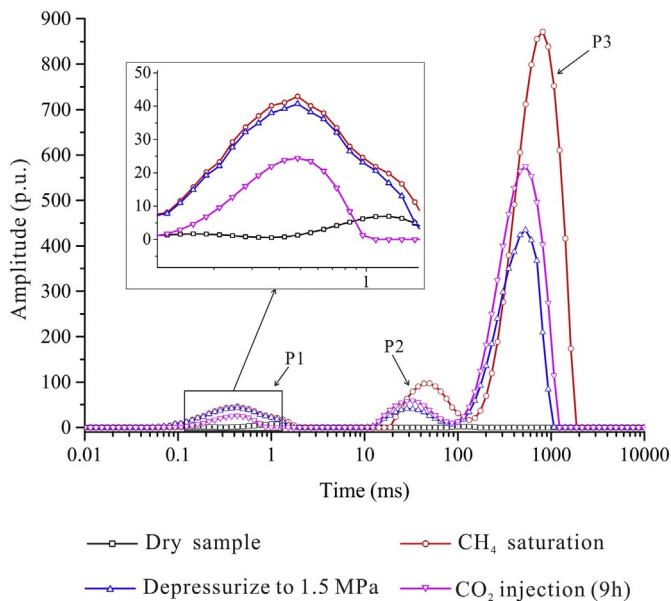


Fig. 12.  $T_2$  spectra of  $CH_4$  in different phases during Process B2.

adsorbed  $CH_4$  in Process A2 were higher than in Process B2 (Fig. 10). In other words, a higher concentration ratio of  $CO_2/CH_4$  improves efficiency for  $CO_2-CH_4$  displacement, assuming all other conditions remain constant. Nevertheless, both at ambient pressure and at the

abandonment pressure, there was a similarly enhanced desorption efficiency (~25%) for the adsorbed methane. This indicates that an additional ~25% of residual gas in the adsorbed phase can be recovered from a depleted shale reservoir with injected  $CO_2$  - with significant implications for the practice and economics of shale gas exploitation.

According to the investigations of the shale gas plays such as the Barnett, Fayetteville, Haynesville Marcellus, and Woodford in USA, the unrecoverable gas of these shale reservoirs is commonly > 90% of original gas in-place (Sandrea, 2012). The average recovery efficiency is about 7%, if only the processes of horizontal drilling and hydrofracturing were implemented (Sandrea, 2012). This study suggests an additional ~25% gas recovery efficiency can be obtained with injected  $CO_2$  than that without  $CO_2$  injection - provided elevated permeabilities of the stressed media may be maintained. Fathi and Akkutlu (2014) ever did a numerical simulation research of 10 years of primary production followed by 5 years of  $CO_2$  injection and 30 years of final production in shale gas reservoirs. Their results indicate that 5 years of  $CO_2$  injection and soaking made the methane recovery increased by 30%, i.e. from 55% in 10 years of primary production to 85% in the 30 years of final production. Although the simulation scenario in Fathi and Akkutlu (2014) is a little different from this study, the simulation results agree well with the experimental results in this study. Both the simulation results and experimental results demonstrate that the injection of  $CO_2$  have great benefit of producing additional adsorbed methane gas in shale gas reservoirs.

This study provides a preliminary experimental evaluation of the recovery of adsorbed  $CH_4$  with  $CO_2$  injection under simplified conditions in the laboratory. In situ reservoir conditions, such as high temperature, water-rock reactions, and other reservoir characteristics are not considered. Moreover, the NMR measurements can also bring some uncertainties in results. First, some hydrogen impurities (remnant methane, hydrocarbon or moisture) may remain in the shale samples even though drying and vacuum extraction are carefully applied before the experiments. Second, the shales may contain some paramagnetic substances such as pyrite. Theoretically, the impurities of both the hydrogen fluids and paramagnetic minerals contained in the shales may add some systematic noise to the NMR measurement. In this study, as shown in Figs. 6, 8, 11 and 12, the spectra curves (black ones) of dry samples are too small, indicating that the level of noise is negligible. We suggest that the method provided in this study is effective in quantitatively evaluating the enhanced recovery of adsorbed-gas resulting from  $CO_2$  injection.

#### 4. Conclusions

We evaluate the exchange of adsorbed and non-adsorbed/free-phase  $CH_4$  during the injection of  $CO_2$ . The method uses low-field NMR spectroscopy to quantitatively identify the adsorbed, porous-medium-confined, and free methane during the experimental processes. Based on a suite of four contrasting injection conditions (pressures and the presence/absence of  $CO_2$ ), the following conclusions are made:

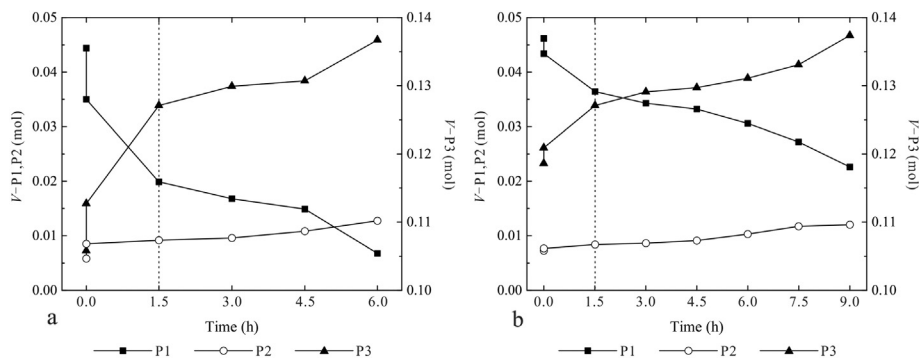


**Fig. 13.** The AOS change of CH<sub>4</sub> in different phase after CO<sub>2</sub> injection. (a), Process A2; (b), Process B2. “0 h” represents NMR measurements taken either before or after the initiation of CO<sub>2</sub> injection. The adsorbed methane volume (P1) is calculated based on Eq. (6); while the non-adsorbed methane volume (P2 and P3) is quantified based on Eq. (3).

Comparing the situations both with and without injected CO<sub>2</sub>, the desorption efficiency of adsorbed CH<sub>4</sub> is enhanced by ~27% and ~26% with CO<sub>2</sub> injection at ambient pressure and abandonment pressure, respectively. An additional ~25% of residual gas in the adsorbed phase can be obtained from a depleted shale reservoir with CO<sub>2</sub> injection. The injected CO<sub>2</sub> can also enhance the PRPH of adsorbed CH<sub>4</sub> by ~11% at ambient pressure and by ~4% at abandonment pressure.

Based on two experiments with CO<sub>2</sub> injection, the higher concentration ratio of CO<sub>2</sub>/CH<sub>4</sub> is more effective for CO<sub>2</sub>-CH<sub>4</sub> displacement, and the CO<sub>2</sub>-CH<sub>4</sub> displacement rate is more rapid during the early CO<sub>2</sub>-CH<sub>4</sub> interaction period.

This study has verified the quantitative capability of NMR-based measurements and methodology to analyze the recovery efficiency of adsorbed CH<sub>4</sub> in shale. In general, this potential for significantly enhanced recovery efficiency of adsorbed methane with CO<sub>2</sub> injection, and its quantification under simple laboratory conditions, suggests considerable promise for CO<sub>2</sub>-EGR in shale gas reservoirs, if the permeability may be retained to access the gas.

## Acknowledgments

We acknowledge financial support from the National Natural Science Foundation of China (41472137), the Foundation for the Author of National Excellent Doctoral Dissertation of PR China (201253), and the Fundamental Research Funds for the Central Universities (2652016120).

## References

- Busch, A., Gensterblum, Y., 2011. CBM and CO<sub>2</sub>-ECBM related sorption processes in coal: a review. *Int. J. Coal Geol.* 87, 49–71.
- Buttler, J.P., Reeds, J.A., Dawson, S.V., 1981. Estimating solution of first kind integral equations with non-negative constraints and optimal smoothing. *SIAM J. Numer. Anal.* 18 (3), 381–397.
- Carr, H.Y., Purcell, E.M., 1954. Effects of diffusion on free precession in nuclear magnetic resonance experiments. *Phys. Rev.* 94 (3), 630–638.
- Chen, Z.W., Liu, J.S., Elsworth, D., Connell, L.D., Pan, Z.J., 2010. Impact of CO<sub>2</sub> injection and differential deformation on CO<sub>2</sub> injectivity under in-situ stress conditions. *Int. J. Coal Geol.* 81, 97–108.
- Chu, S., Majumdar, A., 2012. Opportunities and challenges for a sustainable energy future. *Nature* 488, 294–303.
- Dunn, K.J., LaTorraça, G.A., Warner, J.L., Bergman, D.J., 1994. On the calculation of NMR relaxation time distributions. In: *SPE 69th Annual Technical Conference and Exhibition*, New Orleans, pp. 25–28 (September). SPE. 28367.
- Eshkalak, M.O., Al-shalabi, E.W., Sanaei, A., Aybar, U., Sepehrmoori, K., 2014. Enhanced gas recovery by CO<sub>2</sub> sequestration versus re-fracturing treatment in unconventional shale gas reservoirs. In: *SPE International Petroleum Exhibition and Conference*, Abu Dhabi, pp. 1–18 UAE, 10–13 November. SPE. 172083.
- Fathi, E., Akkutlu, I.Y., 2014. Multi-component gas transport and adsorption effects during CO<sub>2</sub> injection and enhanced shale gas recovery. *Int. J. Coal Geol.* 123, 52–61.
- Fernø, M.A., Hauge, L.P., Uno Rogmo, A., Gautepluss, J., Graue, A., 2015. Flow visualization of CO<sub>2</sub> in tight shale formations at reservoir conditions. *Geophys. Res. Lett.* 42, 7414–7419.
- Fleury, M., Romero-Sarmiento, M., 2016. Characterization of shale using T<sub>1</sub>-T<sub>2</sub> NMR maps. *J. Pet. Sci. Eng.* 137, 55–62.
- Godec, M., Koperna, G., Petrusak, R., Oudinot, A., 2013. Potential for enhanced gas recovery and CO<sub>2</sub> storage in the Marcellus shale in the Eastern United States. *Int. J. Coal Geol.* 118, 95–104.

- Godec, M., Koperna, G., Petrusak, R., Oudinot, A., 2014. Enhanced gas recovery and CO<sub>2</sub> storage in gas shale: a summary review of its status and potential. *Energy Procedia* 63, 5849–5857.
- Goodman, A., Fukai, I., Dilmore, R., Frailey, S., Bromhal, G., Soeder, D., Gorecki, C., Peck, W., Rodosta, T., Guthrie, G., 2014. Methodology for assessing CO<sub>2</sub> storage potential of organic-rich shale formations. *Energy Procedia* 63, 5178–5184.
- Guo, R., Mannhardt, D., Kantzas, A., 2007. Characterizing moisture and gas content of coal by low-field NMR. *J. Can. Petrol. Technol.* 46, 49–54.
- Harrison, R., Falcone, G., 2013. Deciding whether to fund either CCS or CCUS offshore projects: are we comparing apples and pears in the North Sea? In: *SPE Annual Technical Conference and Exhibition*, New Orleans, Louisiana, USA, pp. 1–10 30 September–2 October. SPE. 166388.
- Hazlewood, C.F., Chang, D.C., Nichols, B.L., Woessner, D.E., 1974. Nuclear magnetic resonance transverse relaxation times of water protons in skeletal muscle. *Biophys. J.* 14 (8), 583–606.
- Heller, R., Zoback, M., 2014. Adsorption of methane and carbon dioxide on gas shale and pure mineral samples. *J. Unconv. Oil Gas Resour.* 8, 14–24.
- Li, A., Ding, W.L., Wang, R.Y., He, J.H., Wang, X.H., Sun, Y.X., Gu, Y., Jiao, N.L., 2017. Petrophysical characterization of shale reservoir based on nuclear magnetic resonance (NMR) experiment: a case study of lower Cambrian Qiongzhusi formation in eastern Yunnan province. *South China J. Nat. Gas Sci. Eng.* 37, 29–38.
- Liu, F., Ellett, K., Xiao, Y., Rupp, J.A., 2013. Assessing the feasibility of CO<sub>2</sub> storage in the New Albany Shale (Devonian–Mississippian) with potential enhanced gas recovery using reservoir simulation. *Int. J. Greenh. Gas Control* 17, 111–126.
- Meiboom, S., Gill, D., 1958. Modified Spin-Echo method for measuring nuclear relaxation times. *Rev. Sci. Instr.* 29 (8), 688–691.
- Nuttall, B.C., Eble, C.F., Drahovzal, J.A., Bustin, R.M., 2005. Analyses of Devonian black shales in Kentucky for potential carbon dioxide sequestration and enhanced natural gas production. In: *Kentucky Geological Survey. DOE NETL*, Lexington, Kentucky, USA.
- Rani, S., Prusty, B.K., Pal, S.K., 2015. Methane adsorption and pore characterization of India shale samples. *J. Unconv. Oil Gas Resour.* 11, 1–10.
- Reeves, S.R., 2004. The Coal-Seq project: key results from field, laboratory, and modeling studies. In: *Proc. 7th Conf. Greenhouse Gas Control Technologies* (1399–1403). Elsevier, Oxford.
- Regan, M., 2007. A Review of the Potential for Carbon Dioxide (CO<sub>2</sub>) enhanced gas recovery in Australia. Cooperative Research Centre for Greenhouse Gas Technologies, Canberra (CO<sub>2</sub> CRC Publication. No: RPT07-0802, 39p).
- Sandrea, R., 2012. Evaluating production potential of mature US oil, gas shale plays. *Oil Gas J.* 110, 58–67.
- Schepers, K.C., Nuttall, B.C., Oudinot, A.Y., Gonzalez, R.J., 2009. Reservoir modeling and simulation of the Devonian gas shale of eastern Kentucky for enhanced gas recovery and CO<sub>2</sub> storage. In: *SPE International Conference on CO<sub>2</sub> Capture Storage and Utilization*, San Diego, California, USA, pp. 1–20 10–11 November. SPE. 206620.
- Seevers, D.O., 1966. A nuclear magnetic method for determining the permeability of sandstones. In: *Paper L. SPWLA 7th Annual Logging Symposium*, 9–11 May. Society of Professional Well Log Analysts Transactions, Tulsa, Oklahoma, pp. 1–14.
- Sigal, R.F., Odusina, E., 2011. Laboratory NMR measurements on methane saturated Barnett shale samples. *Petrophysics* 52 (1), 32–49.
- Sun, H., Yao, J., Gao, A.H., Fan, D.Y., Wang, C.C., Sun, Z.X., 2013. Numerical study of CO<sub>2</sub> enhanced natural gas recovery and sequestration in shale gas reservoirs. *Int. J. Greenh. Gas Con.* 19, 406–419.
- Sun, X.X., Yao, Y.B., Liu, D.M., Elsworth, D., Pan, Z.J., 2016. Interactions and exchange of CO<sub>2</sub> and H<sub>2</sub>O in coals: an investigation by low-field NMR relaxation. *Sci Rep* 6, 1–11.
- Vermilyen, J.P., 2011. *Geomechanical Studies of the Barnett Shale*, Texas, USA. PhD dissertation Stanford University, Palo Alto, California, USA.
- Yao, Y.B., Liu, D.M., Che, Y., Tang, D.Z., Tang, S.H., Huang, W.H., 2010. Petrophysical characterization of coals by low-field nuclear magnetic resonance (NMR). *Fuel* 89, 1371–1380.
- Yao, Y.B., Liu, D.M., Xie, S.B., 2014. Quantitative characterization of methane adsorption on coal using a low-field NMR relaxation method. *Int. J. Coal Geol.* 131, 32–40.
- Zhang, G.D., Zhou, W., Ji, S.C., Liu, J.Y., Zhang, J., Yang, H.H., 2015. Experimental study on CO<sub>2</sub> replacement method used in shale gas exploration. *J. Chengdu Univ. Tech.* 42 (3), 366–371 (in Chinese with English abstract).